Ionosphere of Mars during the consecutive solar minima 23/24 and 24/25 as seen by MARSIS-Mars Express

Beatriz Sánchez-Cano, Mark Lester, Marco Cartacci, Roberto Orosei, Olivier Witasse, Pierre-Louis Blelly, Wlodek Kofman

Icarus 393 (2023) 114616

Contents lists available at ScienceDirect

Icarus

journal homepage: www.elsevier.com/locate/icarus

Ionosphere of Mars during the consecutive solar minima 23/24 and 24/25 as seen by MARSIS-Mars Express

Beatriz Sánchez-Cano [a,*], Mark Lester [a], Marco Cartacci [b], Roberto Orosei [c], Olivier Witasse [d], Pierre-Louis Blelly [e], Wlodek Kofman [f,g]

[a] School of Physics and Astronomy, University of Leicester, United Kingdom
[b] Istituto di Astrofisica e Planetologia Spaziali, Istituto Nazionale di Astrofisica, Rome, Italy
[c] Istituto di Radioastronomia, Istituto Nazionale di Astrofisica, Bologna, Italy
[d] ESTEC, European Space Agency, Noordwijk, Netherlands
[e] Institut de Recherche en Astrophysique et Planétologie, CNRS, Toulouse, France
[f] Institut de Planétologie et d'Astrophysique de Grenoble, UGA, CNRS, France
[g] Centrum Badan Kosmicznych Polskiej Akademii Nauk (CBK PAN), Warsaw, Poland

ARTICLE INFO

Keywords:
Mars
Ionosphere
Solar minimum
Solar cycle
Mars express
MARSIS

ABSTRACT

The Mars' ionospheric behavior during two consecutive solar minima (23/24 and 24/25) is investigated with the same dataset. In particular, we use the Mars Advanced Radar for Subsurface and Ionospheric Sounding (MARSIS) on board Mars Express to investigate the total electron content behavior of the whole atmosphere in relation to the solar irradiance (EUV and X-ray fluxes), the solar zenith angle and the heliocentric distance. The topside variability of the electron density profiles is also investigated through variations in the peak density and neutral scale height. Moreover, the equations of the NeMars empirical model of the Martian ionosphere for low solar activity are tested for both minima. We have found that the topside ionosphere of Mars behaved similarly at both solar minima. However, when considering the bottomside, a pronounced reduction in ionization in particular cases is suggested. In addition, larger TEC values are found during the solar minimum 24/25 in the nightside sector that may indicate possible larger plasma transport than during the minimum 23/24. Finally, this study confirms that the ionospheric empirical NeMars model equations derived by Sanchez-Cano et al. (2016) for the low solar activity period during the solar minimum 23/24 are also valid and accurate for the solar minimum 24/25. The long duration of Mars Express is a critical factor for determining the long-term Martian ionospheric variability, which in turn, is essential for understanding the global evolution of the planet's atmosphere.

1. Introduction

The ionosphere of Mars can be considered as a purely photochemical ionosphere mainly formed by O^+ and O_2^+ ions, with a main density layer of $\sim 10^{11}$ m^{-3} peaking at ~135 km near subsolar point, and a secondary density layer of $\sim 10^{10}$ m^{-3} peaking at ~110 km (e.g. Mendillo et al., 2003; Withers, 2009). Both layers are mainly produced by solar radiation, particularly by the extreme-ultraviolet (EUV) and soft X-rays fluxes, respectively (e.g. Withers, 2009; González-Galindo, 2020; Peter et al., 2021). Consequently, Mars' ionosphere follows the pattern of the solar radiation variability, including an ~11-year cycle produced by the cycle of solar activity with a minimum of ionization at the minimum of solar activity, and a maximum of ionization at the maximum of solar activity (e.g. Withers et al., 2015; Sánchez-Cano et al., 2016; Burrell et al., 2020). In addition, Mars' orbit about the Sun is elliptical and has an important effect on the amount of radiation that reaches Mars at each season. This is manifested by a clear annual variation in the ionization on top of the ~11-year variability produced by the solar cycle (e.g. Sánchez-Cano et al., 2015b, 2018). Moreover, this dependence is also seen at higher altitudes. For example, the top of the ionosphere, typically referred as the ionopause, also varies with the EUV flux on annual and solar cycle time scales (Chu et al., 2019) in addition to other factors that also play a role in its formation, such as the magnetic fields and the solar wind dynamic pressure (Sánchez-Cano et al., 2020). Likewise, the Martian bow shock (the most external boundary) also clearly follows this double annual and solar cycle variability and has a strong

* Corresponding author.
E-mail address: bscmdr1@leicester.ac.uk (B. Sánchez-Cano).

https://doi.org/10.1016/j.icarus.2021.114616
Received 1 March 2021; Received in revised form 23 June 2021; Accepted 1 July 2021
Available online 7 July 2021

dependence on the solar flux (Hall et al., 2016a, 2016b; Hall et al., 2019).

Focusing on the effect of the solar cycle at Mars, the ionosphere behaves slightly differently at each phase of the solar cycle as demonstrated by Sánchez-Cano et al. (2015b); Sánchez-Cano et al., 2016) using different Mars Express datasets during the solar cycle 23/24. For instance, significant variability in the distribution of the ionization in the topside profiles was found through the analysis of neutral scale heights for a full solar cycle. In particular, the smallest and more altitude-constant neutral scale heights were found during the low solar activity period in 2007–2010, and the largest and more prominent altitude-dependent scale heights were found during moderate and high solar activity periods (Sánchez-Cano et al., 2015b, 2016). Regarding the scale height dependence with solar zenith angle (SZA), no significant variation was found during the descending and low solar activity phases of the solar cycle, which implies that for these two periods neutral and plasma temperatures had a relatively constant behavior with respect to solar illumination. On the contrary, a linear dependence of the scale heights with SZA was found during the moderate-ascending and high solar activity phases of the solar cycle 23/24, being larger at lower SZA (and so, hotter) and smaller at larger SZA (Sánchez-Cano et al., 2016).

The period that had the most complex ionospheric behavior during the solar cycle 23/24 was the low solar activity phase that occurred between mid-September 2007 to mid-September 2009. This period was characterized by a particularly low level of activity that lasted longer than previous solar minima (e.g., Solomon et al., 2010). Consequently, the lowest level of ionization ever recorded by a mission at Mars was found by Mars Express, which was also seen in a reduction of ~7% of the main peak density (Sánchez-Cano et al., 2016). Particularly remarkable was the notable reduction in the X-ray flux background at Mars that produced a significant reduction in the ionization at the bottomside of the ionosphere (i.e. below the main peak), as well as a frequent absence of the secondary layer (Sánchez-Cano et al., 2016). In addition, the relationship between the solar wind dynamic pressure and the maximum thermal pressure of the ionosphere was the weakest of the solar cycle, leading to a larger probability of finding the topside ionosphere more compressed than at other solar cycle phases, most probably caused by larger penetration of the solar wind draped magnetic field (Sánchez-Cano et al., 2016).

Therefore, the solar minimum of solar cycle 23/24 was unique in many aspects, and it gave us the opportunity to investigate the behavior of the Martian ionosphere under conditions not explored before at Mars. Since we are now at a new minimum of solar activity (solar cycle 24/25), we have the opportunity to investigate whether the Martian ionosphere behaves similarly to the previous solar cycle, or if not, whether the ionospheric behavior of the previous solar minimum may have been unique in that respect. In order to investigate whether this was an exceptional case or a recurrent situation during solar minima, this paper focuses on the analysis of ionospheric data during two consecutive solar minima at Mars, the 23/24 and 24/25 minima, using the same dataset. In particular, we use the Mars Advanced Radar for Subsurface and Ionospheric Sounding (MARSIS) instrument on board Mars Express. This is the first comparison to be done for two consecutive solar minima at Mars with the same dataset, which also has strong implications for ionospheric modelling during the solar cycle.

2. Datasets and ionospheric model used in this study

This study focuses on ionospheric data analysis of the Mars Advanced Radar for Subsurface and Ionospheric Sounding (MARSIS) (Picardi et al., 2004; Orosei et al., 2015) onboard Mars Express (Chicarro et al., 2004) during the two solar minima when Mars Express was in orbit around Mars. The radar has two different operational modes from which different ionospheric information can be retrieved. In particular, we use the total electron content (TEC) from MARSIS when operating in subsurface mode. In this mode, the radar sounds the surface and subsurface of the planet and the TEC is obtained after considering the signal delay introduced by the ionosphere on the radar signals (Safaeinili et al., 2007; Mouginot et al., 2008; Cartacci et al., 2013, 2018; Sánchez-Cano et al., 2015a; Conroy et al., 2019). In this study, we use the TEC algorithm developed by Cartacci et al. (2013); Cartacci et al., 2018). The TEC obtained from the MARSIS subsurface mode represents the total amount of free electrons per unit area found between the spacecraft and the surface of the planet (vertical TEC) but can only be retrieved for high solar zenith angles (SZA) as the radar signals cannot penetrate the dayside ionosphere when it is relatively robust (e.g. Sánchez-Cano et al., 2015a). Therefore, only TEC for SZA $> \sim 55^{\circ}$ are available. Moreover, in order to remove any bad conditioned TEC retrieval, only observations with a signal-to-noise ratio larger than 20 dB are used. A total of 3927 orbits with MARSIS operating in subsurface have been used, which includes a total of 3,783,642 TEC observations. The data distribution with respect to solar longitude (proxy for seasons), time, SZA, latitude and Mars-Sun distance is shown in Fig. 1. Although the data coverage is not the same for both periods, several overlapping regions in latitude, SZA, and solar longitude make the comparisons appropriate. We also use ionospheric data from the MARSIS Active Ionospheric Sounding (AIS) mode (Gurnett et al., 2005; Morgan et al., 2008), where MARSIS works as a topside ionospheric sounder, providing vertical topside electron density profiles from the spacecraft altitude until the peak of the ionosphere (maximum ionization region). In this mode, the signals do not cross the ionosphere below the main peak and so, a larger range of SZAs is available. However, we only use MARSIS-AIS data with SZA between $\sim 50^{\circ}$ and 90° to compare directly with the MARSIS-subsurface TEC observations. In this study, the electron density profile inversions are implemented manually according to Morgan et al. (2013) and Sánchez-Cano et al. (2012). A total of 269 topside electron density profiles from MARSIS operating in AIS have been used, which data coverage is also shown in Fig. 1.

In addition, solar EUV and X-ray irradiance observations from the Thermosphere, Ionosphere, Mesosphere Energetics and Dynamics (TIMED)-Solar EUV Experiment (SEE) satellite (Woods and Eparvier, 2006) are used. These observations are scaled from 1 AU to the Mars heliocentric distance to account for the Mars' orbit evolution under the assumption that solar irradiance levels are homogeneous at all solar longitudes. We note that for long-time series with averaged values (as in this study), this assumption is acceptable, but a recent study by Thiemann et al. (2021) has demonstrated that an uncertainty of about 10 days could be present when extrapolating Earth irradiance data to Mars at large phase angles. We use the 30.5 nm and 9.5 nm wavelengths as the most representative EUV and X-ray wavelengths to ionize the main and secondary layers of the Martian ionosphere, respectively (e.g. Martinis et al., 2003; Fox and Yeager, 2006; Fallows et al., 2015). Level 3 data are used, which includes daily averages after applying corrections for atmospheric absorption, degradation, flare removal, and to 1-AU (https://lasp.colorado.edu/data/timed_see/level3/README_SEE_L3_012.TXT). Moreover, a 27-day running average filter is applied to remove any solar-rotation dependence.

Ionospheric observations at Mars are compared to predictions made by the NeMars model (Sánchez-Cano et al., 2013; Sánchez-Cano et al., 2016). NeMars is a powerful tool to accurately and quickly describe the undisturbed ionosphere of Mars on the same basis as the well-known and widely used NeQuick model for Earth (e.g. Radicella, 2009). It is an empirical model based on MARSIS-AIS data from the solar cycle 23/24, and to a lesser extent on Mars Global Surveyor (MGS) radio science data. It describes the electron density distribution with altitude of the two main ionospheric layers in Mars' ionosphere, as well as peak characteristics, scale heights with respect to solar activity, Sun's distance, seasons, latitude, and local time. The model is widely used, e.g. in support of Mars crosslink radio-occultation between two spacecraft at Mars (Ao et al., 2015; Nava et al., 2020), or to demonstrate the effect of the coma of comet C/2013 A1 (Siding Spring) on Mars (Sánchez-Cano et al., 2020a). In particular, the model is run for the low solar activity

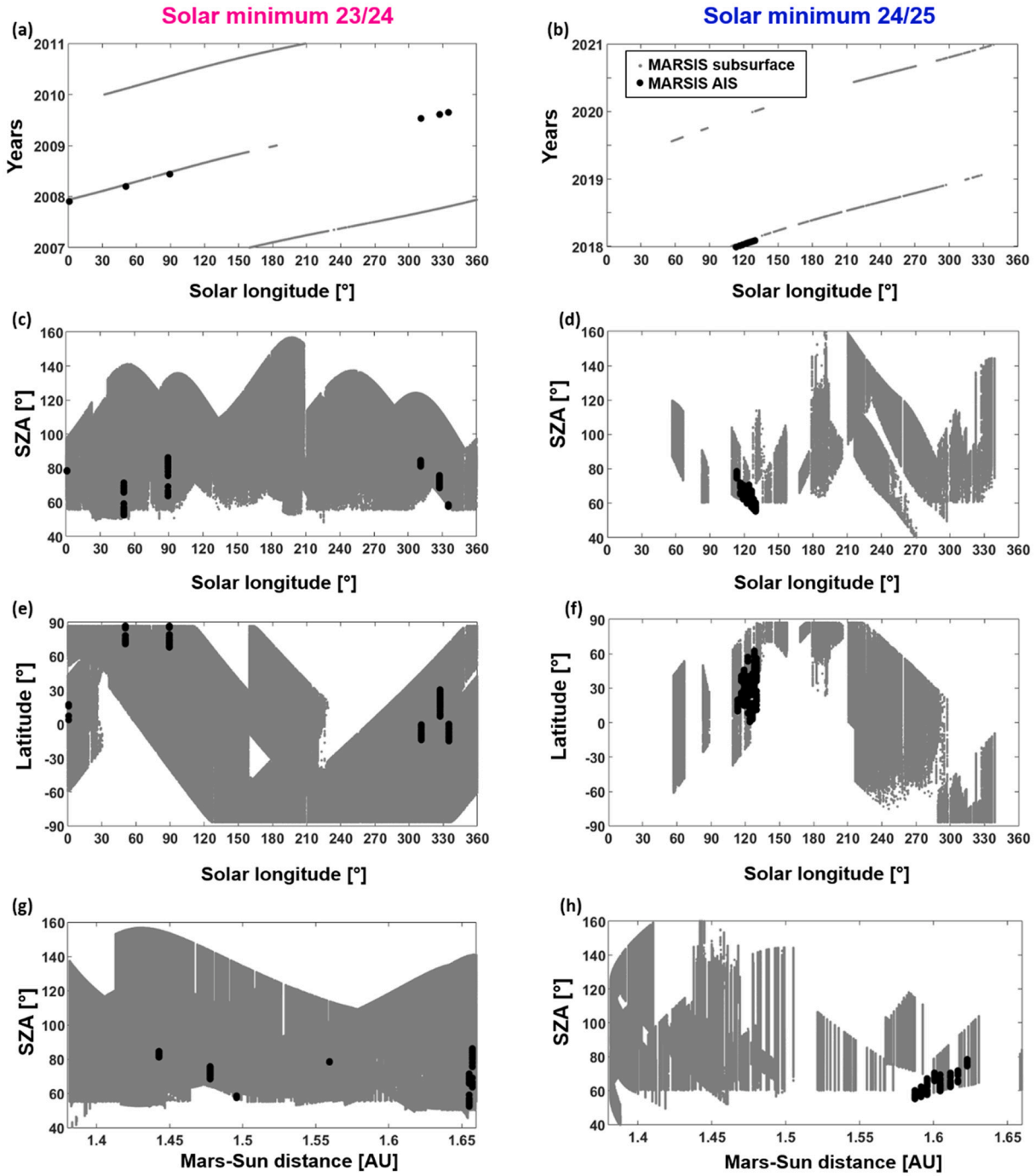

Fig. 1. MARSIS coverage of subsurface data (in grey) and AIS data (in black) used in this study. Left panels refer to solar minimum 23/24 and right panels to solar minimum 24/25. (a,b) Time-Solar longitude. (c,d) Solar Zenith Angle (SZA)-Solar longitude. (e,f) Latitude- Solar longitude. (g,h) Solar Zenith Angle-Mars Sun distance.

conditions described in Sánchez-Cano et al. (2016), which includes the specific neutral scale height derived in that study for the low solar activity period.

3. EUV and X-ray solar fluxes during both solar minima

Fig. 2a–b show the EUV and X-ray TIMED-SEE solar irradiance at 1 AU (in green) and scaled to Mars (in purple), respectively. In general, the solar irradiance is lower at Mars than at 1 AU because it is further from the Sun. The solar cycle variability is clearly seen in both panels with higher fluxes at the maxima of solar activity (~2002 and 2013–2015) and lower fluxes at the minima (2007-mid2010 and 2018–2021). Moreover, the sinusoidal variation seen at Mars' distance is caused by the large ellipticity of the Martian orbit about the Sun, the solar irradiance being higher when Mars is closer to the Sun and lower when further. This annual variation is less visible at both minima in the X-ray fluxes because these wavelengths were largely reduced. For each solar minima, about three terrestrial years are selected that correspond to when the solar irradiance is at the minimum levels at 1 AU. This is because when using fluxes obtained always at the same distance (a circular orbit at 1 AU), the observed irradiance is directly proportional to the Sun's activity, and is not biased by any orbital variability as in

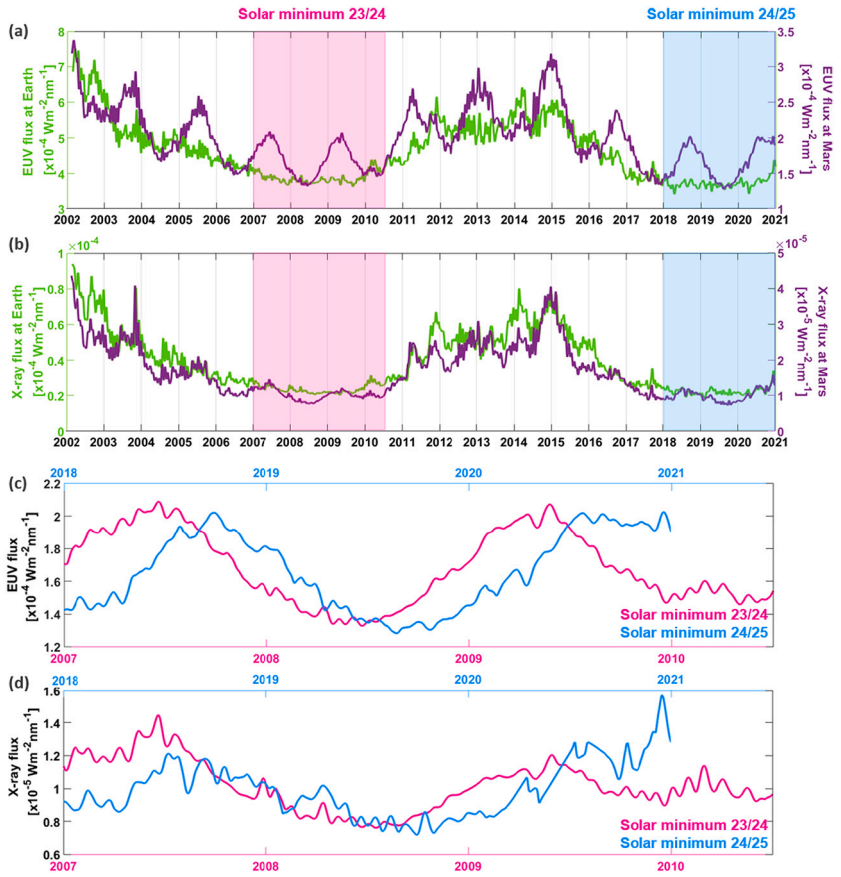

Fig. 2. (a) EUV solar flux at 1 AU in green and scaled to Mars in purple versus time. (b) X-ray solar flux at 1 AU in green and scaled to Mars in purple versus time. In these two panels, the solar minimum 23/24 is marked with a pink box and the solar minimum 24/25 with a blue box. (c, d) Zoom on EUV and X-ray solar fluxes at both solar minima, respectively. (For interpretation of the references to colour in this figure legend, the reader is referred to the web version of this article.)

Mars' case. Therefore, solar minimum 23/24 is identified as data from 2007-mid2010, and solar minimum 24/25 as data from 2018 to 2020, and they are indicated with a pink and blue box in Fig. 2a–b, respectively. This colour scheme is maintained throughout the paper. Fig. 2c–d focus on each solar minimum for the EUV and X-ray solar irradiance scaled to Mars, respectively. In both cases, the solar minimum 23/24 is in pink (bottom abscises) and the solar minimum 24/45 in blue (top abscises). We note that the offset between both profiles is the result of solar minimum starting at different Mars solar longitudes. As can be seen, both minima had similar levels of solar irradiance variability at each wavelength for these two periods at 1 AU. Nevertheless, when looking at similar heliocentric distances some subtle differences can be observed. For example, focusing at the times when the fluxes are the lowest (i.e. Mars furthest from the Sun), the EUV irradiance for the solar minimum 24/25 during the second part of 2019 is lower than the flux on the first part of 2018, as well as during the solar minimum 23/24 in 2008 and 2010. The X-ray flux follows a similar trend although is much reduced for the central part of both minima (2008–2009 and mid2019–2020) than before and after.

4. Total electron content variability

Fig. 3 shows the TEC observations made by MARSIS in subsurface mode with respect to the EUV flux. This is the total number of electrons per unit area found between the spacecraft and the surface of the planet. All the available TEC for both minima have been plotted in four narrow SZA intervals spanning from 65° to 100°. As can be seen, the TEC variability (quantified by standard deviation) is, on average, similar for both solar minima, although the standard deviation is in general larger for the solar minimum 24/25 (blue shaded areas). This means that for the same level of solar irradiance, the ionosphere was slightly more variable during solar minimum 24/25 than during solar minimum 23/24. Moreover, TEC increases linearly with respect to the EUV flux for both minima, corroborating the findings of Sánchez-Cano et al. (2015b) (their Fig. 2) using a subset of MARSIS-AIS topside TEC observations. These authors showed that during the first solar cycle covered by Mars Express (solar cycle 23/24, mid-2005 to mid- 2012), the topside TEC behavior with respect to the EUV flux for SZAs between 45° and 55° had a small increase with increasing EUV in contrast to the significant increasing trend found at moderate and high solar activity periods. In our case, the TEC of both solar minima also show a similar response to the EUV flux and indicates that a similar trend also occurs for larger SZAs.

In order to investigate the effect of the Mars-Sun distance on the ionosphere, Fig. 4a-4d shows the mean TEC value per SZA (solid lines) and their standard deviations (shades areas). The main difference between these panels is that only data from the most extreme heliocentric distances have been plotted. This is 1.38 AU on panels (a) and (c) and 1.66 AU on panels (b) and (d). As expected, the TEC is larger for lower SZA (dayside), decreases toward the terminator (SZA = 90°), and is maintained at a low level on the nightside mainly by plasma transport (SZA > 90°). Also, the TEC is lower (higher) at furthest (closer) distances from the Sun because the level of solar irradiance that reaches Mars varies along the orbit (Fig. 2). The absolute differences of these TEC-SZA curves for both solar minima at the same distances are plotted as solid black lines in panels (e) and (f), respectively. It is found that for the furthest Mars-Sun distance (1.66 AU), the TEC variability during both solar minima is mostly the same as the absolute difference of their means

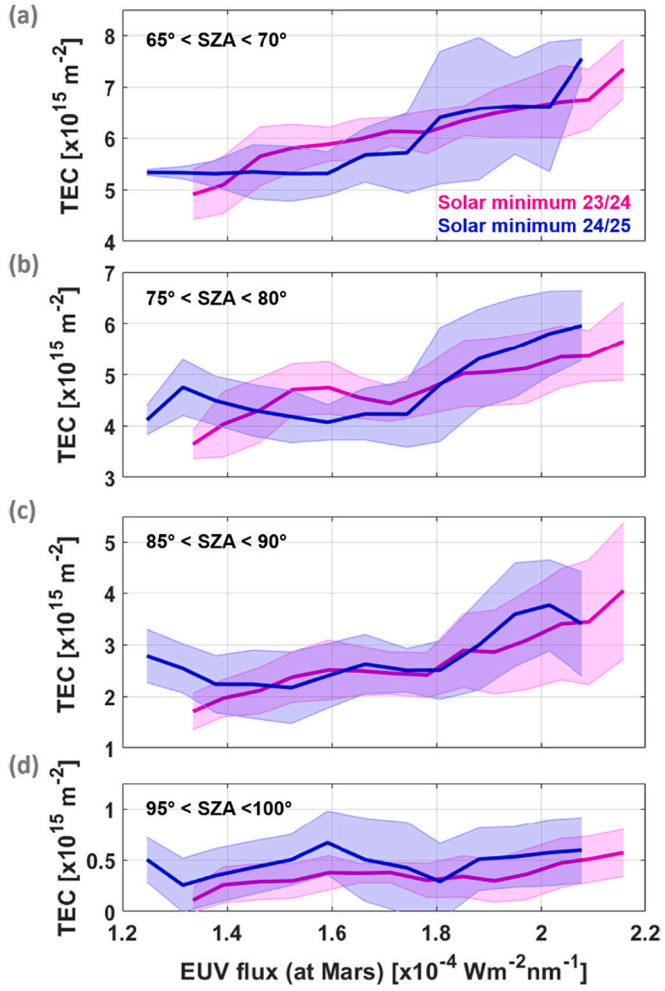

Fig. 3. TEC variation with respect to EUV solar flux at Mars' distance for four narrow intervals of solar zenith angle (SZA). The mean averages are plotted as solid lines and the standard deviation as shaded areas for the solar minimum 23/24 (in pink) and 24/25 (in blue). All EUV intervals have more than 40 data points, except the first data point in panel (a) blue curve that includes only 8 data points. (For interpretation of the references to colour in this figure legend, the reader is referred to the web version of this article.)

is $<4 \times 10^{14}$ m^{-2} on the dayside (<5%). There is only a small difference for the nightside sector (SZA > 90°) where the TEC during the solar minimum 24/25 is larger indicating a possible larger plasma transport than during the minimum 23/24. On the contrary, for the closest Mars-Sun distance (1.38 AU), the TEC during solar minimum 24/25 is, on average, higher than for the minimum 23/24 for all SZA, being particularly remarkable on the dayside (SZA < 90°, $<6 \times 10^{14}$ m^{-2} difference), while near no difference on the nightside is found (SZA > 90°). Since the data coverage is different for each minima, the total number of available observations per degree of SZA is plotted on panels (g) and (h). Although there are more observations for the solar minimum 23/24 than for solar minimum 24/25, the amount of data is sufficient in both cases to perform the comparison (for SZA > 60°). Finally, in order to estimate the degree of variability according to the expected ionosphere for solar steady conditions, Fig. 4a–d shows also the NeMars model that has been used to plot the estimated TEC of the Martian ionosphere for the same solar irradiance (taken as F10.7 flux) and heliocentric conditions of both periods. Although the model gives the TEC of the ionosphere between 100 and 400 km rather than for the full atmosphere, the majority of the TEC is expected to come from the area close to the maximum ionization region (~120–140 km). Therefore, the NeMars TEC can be considered as a proxy for the total TEC of the entire atmospheric column. In addition, we note that the model can only be run for the dayside ionosphere (SZA < 90°), and in particular the model has been run for the SZA interval between 50° and 85°.

For the closest Mars-Sun distance (1.38 AU), the model reproduces well the measured TEC, particularly for the solar minimum 24/25. The solar minimum 23/24 is also well reproduced by the model when considering the errorbars, although the average value is slightly lower than the model predictions. For the further Mars-Sun distance (1.66 AU), TEC at both solar minima are of the order of ~16% lower than the model prediction. These variations imply that there are some differences between the bottomside of the actual ionosphere and the model because the topside of the model (i.e. the neutral scale height) is based on MARSIS-AIS data from the solar minimum 23/24 (Sánchez-Cano et al., 2016) as will be discussed in the next Section. In fact, this previous study found that a large reduction of the X-ray flux during solar minimum 23/24 significantly reduced the bottomside of the ionosphere, which was corroborated with electron density profiles from the radio science instrument on board Mars Express (Sánchez-Cano et al., 2016). Moreover, the typical contribution of the bottomside ionosphere to the total TEC is of that order (Sánchez-Cano et al., 2015a). Therefore, the discrepancy between the model and the actual data in Fig. 4 may indicate a systematic reduction of the bottomside ionosphere during both solar minima. This bottomside reduction may have not affected the TEC during the solar minimum 24/25 at the closest distances to the Sun (i.e. 1.38 AU) as the model and data agree well.

5. Topside ionosphere

In order to corroborate the findings of Section 4, the topside ionospheric profile is also investigated. In this case, the study focuses on MARSIS-AIS topside electron density profiles and how they compare with respect to the NeMars model estimates. An important aspect to consider for the comparisons between solar minimum and the model is whether the density of the main peak of the ionosphere (N_{max}) was similar at both solar minimum. This is important because a difference in the peak density of both minima could produce a bias in the comparisons at higher altitudes. Sánchez-Cano et al. (2016) found that a reduction of the ~7% of the main peak density was present during the solar minimum 23/24 compared to the NeMars estimates. In order to check whether this also occurred at the solar minimum 24/25, Fig. 5a–b shows the relationship of each solar minima peak densities with respect to the model estimates. Note that the model takes into account the 7% reduction previously observed for both minima. As can be seen, data in both panels can be reproduced with the model, indicating that both solar minima had similar levels of peak density values.

Regarding the density variation with altitude within a profile, the data and model are compared in Fig. 5c–f. To compare profiles obtained with different SZA conditions, we first need to remove the SZA dependence. For that, the profiles are normalized following the criteria used in Sánchez-Cano et al. (2015b). This normalization consists of dividing the observed electron density (N) by the peak electron density (N_{max}) of each profile, and subtracting the observed altitude (h) by the peak altitude (h_{max}) of each profile and then dividing it by the observed neutral scale height (H_{max}) of the profile in the peak region (see Eq. (1)).

$$\frac{N}{N_{max}} \; and \; \frac{h - h_{max}}{H_{max}} \tag{1}$$

In turn, H_{max} is obtained by numerically fitting each individual profile to an α-Chapman layer (Chapman, 1931) where the scale height is described using Eq. (2) (as in Sánchez-Cano et al., 2013).

$$H = H_{max} + a(h - h_{max}) \tag{2}$$

where H is the neutral scale height of the entire profile, and a is the normalization factor that reflects the dependence degree of H with h.

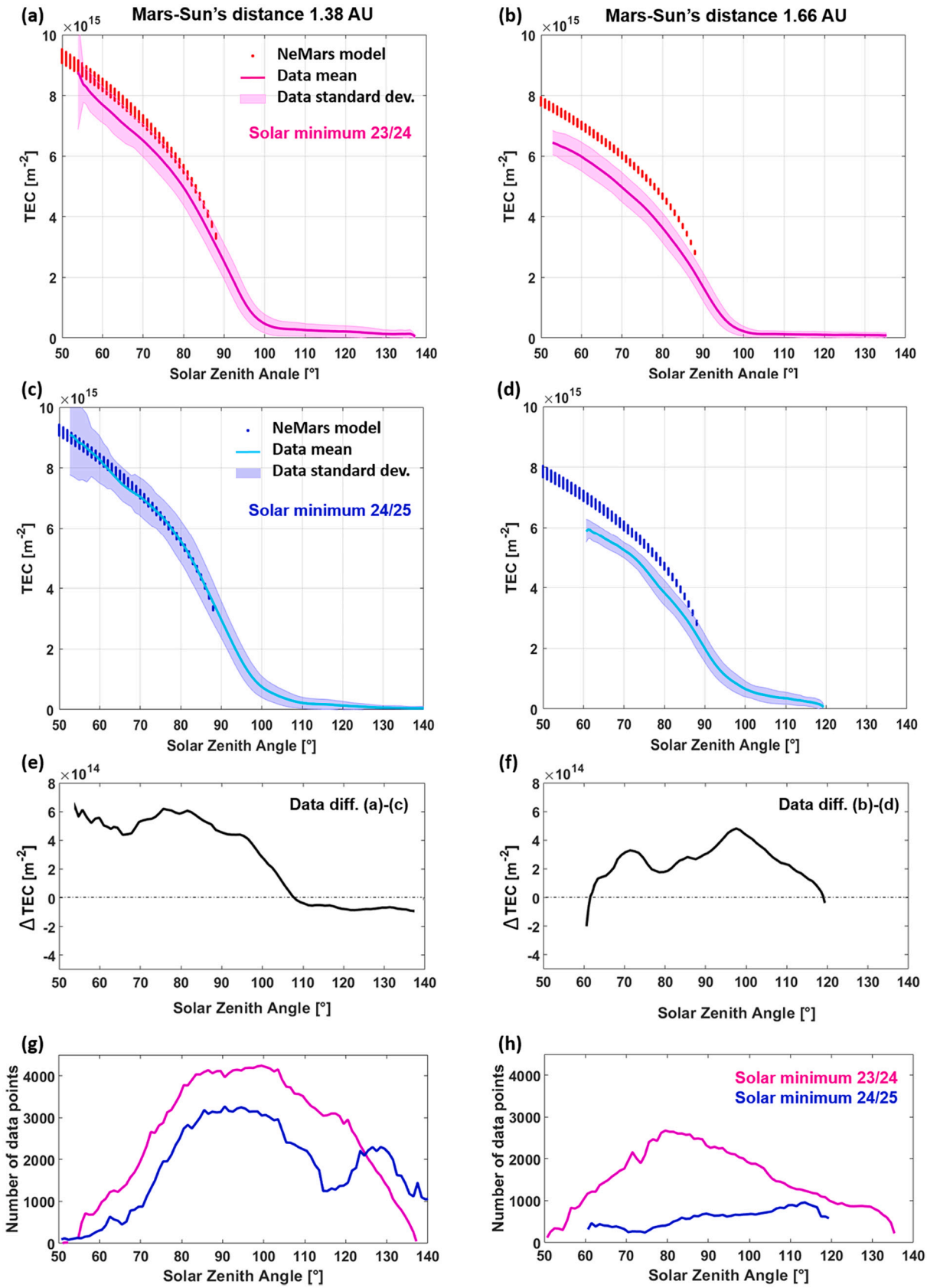

Fig. 4. (a–d) Total electron content (TEC) versus solar zenith angle (SZA) (data and NeMars model outputs) for the solar minimum 23/24 (in pink) and 24/25 (in blue) and for heliocentric distances of 1.38 AU and 1.66 AU (left and right panels, respectively). Mean data values are plotted as a solid line and the standard deviation as shaded areas. The NeMars model is plotted as dots. (e,f) Mean absolute difference between data from solar minimum 24/25 and solar minimum 23/24 for same heliocentric distances. (g,h) Total number of observations for each respective solar minima calculated every degree of solar zenith angle. (For interpretation of the references to colour in this figure legend, the reader is referred to the web version of this article.)

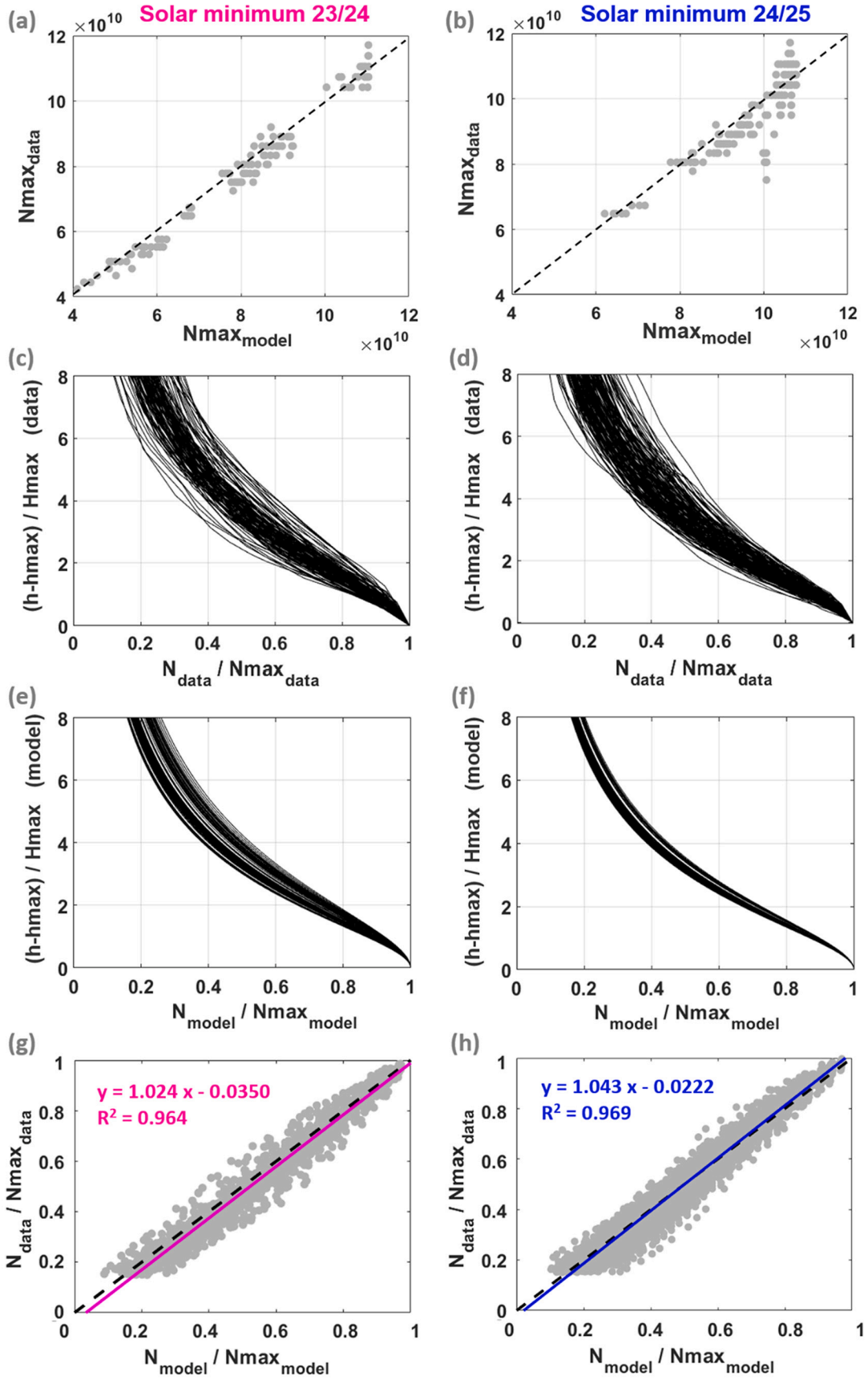

(caption on next page)

Fig. 5. Left panels refer to solar minimum 23/24 and right panels to solar minimum 24/25. (a,b) Peak electron density comparison between data and model. The 1:1 relationship is indicated with a black dashed line. (c,d) MARSIS-AIS topside normalized electron density profiles of the photochemical region. (e,f) NeMars topside normalized electron density profiles for the same conditions of panels c and d, respectively. (g,h) Relationship between the normalized topside electron density observations of the photochemical region only (in panels c and d) and the model reference density (in panels e and f), respectively, for the same normalized altitudes. In each panel, the relation 1:1 is indicated with a black dashed line and the current linear best fit in solid pink for solar minimum 23/24 and solid blue for solar minimum 24/25. The best-fit equations and R^2 are also included. (For interpretation of the references to colour in this figure legend, the reader is referred to the web version of this article.)

After each numerical fit, H_{max} is acquired for each AIS topside electron density profile. We note that this normalization is only valid for the photochemical region of the ionosphere, and so, only data below 200 km are considered. The resulting normalized profiles for the photochemical region are shown in Fig. 5c and d.

In order to compare these profiles also with model results, the NeMars model is run for the same conditions of the observed profiles in Fig. 5, and the same normalization procedure is applied to the modelled profiles. The resulting normalized model-profiles are shown in Fig. 5e and f. As can be seen, in general, they give a similar response to the actual profiles in panels (c) and (d).

The observed-model profile comparisons are shown in Fig. 5g and h, where the relationships between both normalized profiles are shown for both minima. This comparison reflects the degree of variation that the neutral scale height (H) has at both minima with respect to the model, as this parameter describes the shape of the profile and how the ionization varies with altitude. We have plotted the data-normalized density versus the model-normalized density for the same normalized altitudes (every 0.08 step in altitude). A value of 1 corresponds to data comparison near the peak of the ionosphere and lower values correspond to data at higher altitudes (same as in Fig. 5c and f in abscises). If the data points follow the 1:1 relationship, it indicates that the model properly reproduces the observations. As can be seen, the best linear fit to both datasets gives a robust result that is very close to the 1:1 relationship between the data and the model. Consequently, this figure confirms that the NeMars model for low solar activity conditions (particularly the neutral scale height) reproduces very well the topside of the ionosphere of Mars for both solar minima under a broad range of F10.7 flux, SZA and Mars-Sun distance conditions, and so, the empirical equations developed in Sánchez-Cano et al. (2016) are valid for both periods. Furthermore, it also indicates that the topside ionosphere during the two solar minima was similar and that the differences observed in Fig. 4 are mainly produced by changes in the bottomside of the ionosphere.

6. Discussion

The ionosphere of Mars is known to show large variability (e.g. Mendillo et al., 2017; Sánchez-Cano et al., 2015b; Sánchez-Cano et al., 2016), especially during low activity phases of the solar cycle. We have shown that during the latest two solar minima (23/24 and 24/25), the amount of solar radiation that reached Mars was relatively similar and so, the ionosphere behaved on a similar way. In particular, the topside ionosphere shows almost no variation between both solar minima, which guarantees that the empirical equations derived from the solar minima 23/24 for the NeMars model are valid for the solar minima 24/25.

Regarding the general trend of the total TEC with respect to SZA of the atmosphere, it is in general as predicted by the model. The NeMars model assumes the bottomside is described by an α-Chapman layer. Although the TEC model results match the data within the errorbars (standard deviation), we note that there are some TEC reductions of up to about 16% of the data that can be explained by a reduction on the ionization of the bottomside ionosphere. This model-data discrepancy could be caused by the uncertainty of both the model and datasets. The model has been extensively tested with observations from the solar cycle 23/24 and this is the first time that it has been tested with data from the solar cycle 24/25. Previous work indicated that the mean and median differences with respect to independent AIS observations (not used to build the model) are below 3.5% for the electron density and below 1% for the altitude, while the electron density standard deviation is typically below 6% and below 8% for the altitude (Sánchez-Cano et al., 2013; Sánchez-Cano et al., 2015a). For the TEC, which is obtained by integration of the electron density profile with altitude, this is below 5%. Therefore, the uncertainty of the model is lower than the difference observed between the two minima at close distances to the Sun. Regarding the datasets, several algorithms have historically produced different estimates of the TEC retrieved when MARSIS operates in the subsurface mode (Safaeinili et al., 2007; Mouginot et al., 2008; Cartacci et al., 2013, 2018; Conroy et al., 2019). In particular, Sánchez-Cano et al. (2015a) undertook a critical assessment of the different algorithms finding that for SZA $> 75^\circ$ all of them agree well. However, the main differences appeared for SZA $< 75^\circ$. After that, Cartacci et al. (2018) revisited their algorithm in order to solve an issue on their former algorithm described in Cartacci et al. (2013), which produced an overestimate of TEC estimates on the dayside. Despite any possible remaining dayside differences on the TEC magnitude, several studies have shown that both TEC algorithms are appropriate for science, especially at large SZA and for temporal variability studies, as is the case of this work (e.g. Lillis et al., 2010; Mendillo et al., 2013; Sánchez-Cano et al., 2018; Bergeot et al., 2019; Burrell et al., 2020). Moreover, these studies have proven that the science done with both algorithms is complementary. Therefore, since we are using the same dataset for the comparison of the ionospheric variability during both minima, and most of the available data come in any case from large solar zenith angles, we consider that the use of the Cartacci et al. (2018) algorithm for the TEC is appropriate.

In addition, it is also well known that the bottomside ionosphere is very variable as recently demonstrated by Peter et al. (2021) using 14 years of Mars Express radio science data. Although the X-ray flux is responsible for the majority of the ionization in this region, secondary electrons are also known to have an important ionization role. Moreover, it is also known to be strongly affected by sporadic layers during meteoritic ablation (Whalley and Plane, 2010), or intense space weather activity (Sánchez-Cano et al., 2019). Therefore, it is expected that a reduction in the X-ray flux during solar minima might have an effect on the ionization of the bottomside, although not on a constant basis due to the other many phenomena that affect this region. One of these possible factors is the larger TEC variability observed with irradiance for the second solar minimum. Another aspect to consider is that the TEC reduction could be caused by lower ionization at altitudes above 200 km (at the diffusion region of the ionosphere). Nevertheless, the electron density above 200 km is very low, and so, the TEC contribution of this region to the total TEC can be considered negligible.

7. Conclusions

We have performed the first comparison of two consecutive solar minima at Mars with the same dataset. We have found:

- The ionosphere of Mars behaved, in general, very similar at both solar minima. Despite the extended low solar irradiance of the solar minimum 23/24, the largely reduced ionization found at Mars during that period might be the typical behavior of the ionosphere during any solar minimum.
- The TEC increases linearly with respect to EUV for all SZA at both minima.

- The TEC versus SZA behavior is similar for both solar minima at large Mars-Sun distances and about ~16% lower than the model prediction. However, for closer Mars-Sun distances, the model reproduces very well the TEC behavior for the minimum 24/25, but to some extent overestimates the TEC for the minimum 23/24.
- The topside ionosphere behaved similar for both minima and as predicted by the NeMars model.
- A pronounced reduction of the bottomside ionosphere during the first solar minimum and also during both minima at further distances may have occurred.
- Larger TEC values are found during the solar minimum 24/25 in the nightside sector that may indicate possible larger plasma transport than during the minimum 23/24.
- Finally, an important output of this study is the confirmation that the ionospheric empirical model equations derived by Sánchez-Cano et al. (2016) for the low solar activity period during the solar minimum 23/24 are also valid and can be extrapolated to the solar minimum 24/25.

This study has only been possible thanks to the long duration of Mars Express, which is a critical factor for understating the long-term Martian ionospheric variability, which in turn, is essential for understanding the global evolution of the planet's atmosphere.

Declaration of Competing Interest

None.

Acknowledgments

B.S.-C and M.L. acknowledge support through UK-STFC Grant ST/S000429/1. M.C. acknowledges support from the Italian Space Agency (ASI) through contract ASI-INAF 2019–21-HH.0. MARSIS-MEX data are freely available at https://www.cosmos.esa.int/web/psa/mars-express, and TIMED-SEE data at the University of Colorado's website (https://lasp.colorado.edu/lisird/data/timed_see_ssi_l3/).

References

Ao, C.O., Edwards, C.D., Kahan, D.S., Pi, X., Asmar, S.W., Mannucci, A.J., 2015. A first demonstration of Mars crosslink occultation measurements. Radio Sci. 50, 997–1007. https://doi.org/10.1002/2015RS005750.

Bergeot, N., Witasse, O., Le Maistre, S., Blelly, P.-L., Kofman, W., Peter, K., Dehant, V., Chevalier, J.-M., 2019. MoMo: a new empirical model of the Mars ionospheric total electron content based on Mars Express MARSIS data. J. Space Weather Space Clim. 9, A36 https://doi.org/10.1051/swsc/2019035.

Burrell, A.G., Sánchez-Cano, B., Witasse, O., Lester, M., Cartacci, M., 2020. Comparison of terrestrial and Martian TEC at Dawn and Dusk during solstices. Earth Planet. Space 72, 140. https://doi.org/10.1186/s40623-020-01258-3.

Cartacci, M., Amata, E., Cicchetti, A., Noschese, R., Giuppi, S., Langlais, B., Frigeri, A., Orosei, R., Picardi, G., 2013. Mars ionosphere total electron content analysis from MARSIS subsurface data. Icarus 223 (1), 423–437. https://doi.org/10.1016/j.icarus.2012.12.011.

Cartacci, M., Sánchez-Cano, B., Orosei, R., Noschese, R., Cicchetti, A., Witasse, O., Cantini, F., Pio Rossi, A., 2018. Improved estimation of Mars ionosphere total electron content. Icarus 299, 396–410. https://doi.org/10.1016/j.icarus.2017.07.033.

Chapman, S., 1931. The absorption and dissociative or ionizing effect of monochromatic radiation in an atmosphere on a rotating earth. Proc. Phys. Soc. (Lond.) 43, 26–45.

Chicarro, A., Martin, P., Traunter, R., 2004. Mars Express: A European Mission to the Red Planet SP-1240. Eur. Space Agency Publ. Div., Noordwijk, Netherlands, pp. 3–16.

Chu, F., Girazian, Z., Gurnett, D.A., Morgan, D.D., Halekas, J., Kopf, A.J., Thiemann, E.M. B., Duru, F., 2019. The effects of crustal magnetic fields and solar EUV flux on ionopause formation at Mars. Geophys. Res. Lett. 46, 10,257–10,266. https://doi.org/10.1029/2019GL083499.

Conroy, P., Quinsac, G., Floury, N., Witasse, O., Cartacci, M., Orosei, R., Kofman, W., Sánchez-Cano, B., 2019. A new method for determining the total electron content in Mars' ionosphere based on Mars express MARSIS data. Planet. Space Sci. 182, 104812. https://doi.org/10.1016/j.pss.2019.104812.

Fallows, K., Withers, P., Matta, M., 2015. An observational study of the influence of solar zenith angle on properties of the M1 layer of the Mars ionosphere. J. Geophys. Res. Space Phys. 120, 1299–1310. https://doi.org/10.1002/2014JA020750.

Fox, J.L., Yeager, K.E., 2006. Morphology of the near-terminator Martian ionosphere: a comparison of models and data. J. Geophys. Res. 111, A10309 https://doi.org/10.1029/2006JA011697.

González-Galindo, F., 2020. Martian Ionospheric Observation and Modelling. Oxford Research Encyclopedia of Planetary Science. https://oxfordre.com/planetaryscience/view/10.1093/acrefore/9780190647926.001.0001/acrefore-9780190647926-e-79.

Gurnett, D.A., et al., 2005. Radar soundings of the ionosphere of Mars. Science 310, 1933–1999. https://doi.org/10.1126/science.1121868.

Hall, B.E.S., Lester, M., Nichols, J., Sánchez-Cano, B., Andrews, D., Opgenoorth, H., Fränz, M., 2016a. A survey of superthermal electron flux depressions, or 'electron holes', within the illuminated Martian induced magnetosphere. J. Geophys. Res. Space Phys. 121, 4835–4857. https://doi.org/10.1002/2015JA021866.

Hall, B.E.S., Lester, M., Sánchez-Cano, B., Nichols, J.D., Andrews, D.J., Edberg, N.J.T., Opgenoorth, H.J., Fränz, M., Holmström, M., Ramstad, R., Witasse, O., Cartacci, M., Cicchetti, A., Noschese, R., Orosei, R., 2016b. Annual variations in the Martian bow shock location as observed by the Mars Express mission. J. Geophys. Res. Space Physics 121, 11,474–11,494. https://doi.org/10.1002/2016JA023316.

Hall, B.E.S., Sánchez-Cano, B., Wild, J., Lester, M., Holmstrom, M., 2019. The Martian bow shock over solar cycle 23-24 as observed by the Mars Express mission. J. Geophys. Res. Space Physics 124, 4761–4772. https://doi.org/10.1029/2018JA026404.

Lillis, R.J., Brain, D.A., England, S.L., Withers, P., Fillingim, M.O., Safaeinili, A., 2010. Total electron content in the Mars ionosphere: temporal studies and dependence on solar EUV flux. J. Geophys. Res. 115, A11314 https://doi.org/10.1029/2010JA015698.

Martinis, C.R., Wilson, J.K., Mendillo, M.J., 2003. Modeling day-to-day ionospheric variability on Mars. J. Geophys. Res. 108, 1383. https://doi.org/10.1029/2003JA009973.

Mendillo, M., Smith, S., Wroten, J., Rishbeth, H., Hinson, D., 2003. Simultaneous ionospheric variability on Earth and Mars. J. Geophys. Res. 108 (1432), A12. https://doi.org/10.1029/2003JA009961.

Mendillo, M., Narvaez, C., Withers, P., Matta, M., Kofman, W., Mouginot, J., 2013. Variability in ionospheric total electron content at Mars. Planet. Space Sci. 86, 117–129. https://doi.org/10.1016/j.pss.2013.08.010.

Mendillo, M., Narvaez, C., Vogt, M.F., Mayyasi, M., Forbes, J., Galand, M., Andersson, L., 2017. Sources of ionospheric variability at Mars. J. Geophys. Res. Space Physics 122, 9670–9684. https://doi.org/10.1002/2017JA024366.

Morgan, D.D., Gurnett, D.A., Kirchner, D.L., Fox, J.L., Nielsen, E., Plaut, J.J., 2008. Variation of the Martian ionospheric electron density from Mars Express radar soundings. J. Geophys. Res. 113, A09303 https://doi.org/10.1029/2008JA013313.

Morgan, D.D., Witasse, O., Nielsen, E., Gurnett, D.A., Duru, F., Kirchner, D.L., 2013. The processing of electron density profiles from the Mars Express MARSIS topside sounder. Radio Sci. 48, 197–207. https://doi.org/10.1002/rds.20023.

Mouginot, J., Kofman, W., Safaeinili, A., Herique, A., 2008. Correction of the ionospheric distortion on the MARSIS surface sounding echoes. Planet. Space Sci. 56, 917–926. https://doi.org/10.1016/j.pss.2008.01.010.

Nava, B., Kashcheyev, A., Migoya-Orue, Y., Radicella, S.M., Parrott, J., Sánchez-Cano, B., Witasse, O., Svedhem, H., Titov, D., Ao, C.O., 2020. Mutual radio occultation experiment between ExoMars Trace Gas Orbiter and Mars Express: Feasibility study and preparation for the data analysis. In: 14th Europlanet Science Congress 2020, held virtually, 21 September 2020–9 October, 2020. Online at.

Orosei, R., Jordan, R.L., Morgan, D.D., Cartacci, M., Cicchetti, A., Duru, F., Gurnett, D.A., Heggy, E., Kirchner, D.L., Noschese, R., Kofman, W., Masdea, A., Plaut, J.J., Seu, R., Watters, T.R., Picardi, G., 2015. Mars Advanced Radar for Subsurface and Ionospheric Sounding (MARSIS) after nine years of operation: a summary. Planet. Space Sci. 112, 98–114. https://doi.org/10.1016/j.pss.2014.07.010.Peter.

Peter, K., Pätzold, M., Molina-Cuberos, G.J., González-Galindo, F., Witasse, O., Tellmann, S., Häusler, B., Bird, M.K., 2021. The lower dayside ionosphere of Mars from 14 years of MaRS radio science observations. Icarus 359, 114213. ISSN 0019-1035. https://doi.org/10.1016/j.icarus.2020.114213.

Picardi, G., et al., 2004. Mars Express: A European Mission to the Red Planet, MARSIS: Mars Advanced Radar for Subsurface and Ionosphere Sounding SP-1240. Eur. Space Agency Publ. Div., Noordwijk, Netherlands, pp. 51–70.

Radicella, S.M., 2009. The NeQuick model genesis, uses and evolution. Ann. Geophys. 52 (3–4), 417–422. https://doi.org/10.4401/ag-4597 [S.l.]. ISSN 2037-416X.

Safaeinili, A., Kofman, W., Mouginot, J., Gim, Y., Herique, A., Ivanov, A.B., Plaut, J., Picardi, G., 2007. Estimation of the total electron content of the Martian ionosphere using radar sounder surface echoes. Geophys. Res. Lett. 34, L23204 https://doi.org/10.1029/2007GL032154.

Sánchez-Cano, B., Witasse, O., Herraiz, M., Radicella, S.M., Bauer, J., Blelly, P.-L., Rodríguez-Caderot, G., 2012. Retrieval of ionospheric profiles from the Mars Express MARSIS experiment data and comparison with radio-occultation data. Geosci. Instrum. Method Data Syst. 1, 77–84. https://doi.org/10.5194/gi-1-77-2012.

Sánchez-Cano, B., Radicella, S.M., Herraiz, M., Witasse, O., Rodríguez-Caderot, G., 2013. NeMars: an empirical model of the Martian dayside ionosphere based on Mars Express MARSIS data. Icarus 225, 236–247. https://doi.org/10.1016/j.icarus.2013.03.021.

Sánchez-Cano, B., et al., 2015a. Total electron content in the Martian atmosphere: a critical assessment of the Mars Express MARSIS data sets. J. Geophys. Res. Space Phys. 120, 2166–2182. https://doi.org/10.1002/2014JA020630.

Sánchez-Cano, B., Lester, M., Witasse, O., Milan, S.E., Hall, B.E.S., Blelly, P.-L., Radicella, S.M., Morgan, D.D., 2015b. Evidence of scale height variations in the Martian ionosphere over the solar cycle. J. Geophys. Res. Space Physics 120, 10,913–10,925. https://doi.org/10.1002/2015JA021949.

Sánchez-Cano, B., Lester, M., Witasse, O., Milan, S.E., Hall, B.E.S., Cartacci, M., Peter, K., Morgan, D.D., Blelly, P.L., Radicella, S., Cicchetti, A., Noschese, R., Orosei, R., Pätzold, M., 2016. Solar cycle variations in the ionosphere of Mars as seen by multiple Mars express data sets. J. Geophys. Res. Space Physics 121, 2547–2568. https://doi.org/10.1002/2015JA022281.

Sánchez-Cano, B., Lester, M., Witasse, O., Blelly, P.-L., Indurain, M., Cartacci, M., González-Galindo, F., Vicente-Retortillo, Á., Cicchetti, A., Noschese, R., 2018. Spatial, seasonal, and solar cycle variations of the Martian total electron content (TEC): is the TEC a good tracer for atmospheric cycles? J. Geophys. Res. 123, 1746–1759. https://doi.org/10.1029/2018JE005626.

Sánchez-Cano, B., Blelly, P.-L., Lester, M., Witasse, O., Cartacci, M., Orosei, R., et al., 2019. Origin of the extended Mars radar blackout of September 2017. J. Geophys. Res. Space Physics 124, 4556–4568. https://doi.org/10.1029/2018JA026403.

Sánchez-Cano, B., Lester, M., Witasse, O., Morgan, D.D., Opgenoorth, H., Andrews, D.J., et al., 2020a. Mars' ionospheric interaction with comet C/2013 A1 siding spring's coma at their closest approach as seen by Mars Express. J. Geophys. Res. Space Phys. 125, e2019JA027344 https://doi.org/10.1029/2019JA027344.

Sánchez-Cano, B., Narvaez, C., Lester, M., Mendillo, M., Mayyasi, M., Holmstrom, M., et al., 2020b. Mars' ionopause: a matter of pressures. J. Geophys. Res. Space Phys. 125, e2020JA028145 https://doi.org/10.1029/2020JA028145.

Solomon, S.C., Woods, T.N., Didkovsky, L.V., Emmert, J.T., Qian, L., 2010. Anomalously low solar extreme-ultraviolet irradiance and thermospheric density during solar minimum. Geophys. Res. Lett. 37, L16103 https://doi.org/10.1029/2010GL044468.

Thiemann, E.M.B., Eparvier, F.G., Knoer, V., Al Muharrami, A., Lillis, R.J., 2021. Solar EUV irradiance uncertainties for planetary studies. J. Geophys. Res. Space Phys. 126, e2020JA028184 https://doi.org/10.1029/2020JA028184.

Whalley, C.L., Plane, J.M.C., 2010. Meteoric ion layers in the Martian atmosphere. Faraday Discuss. 147, 349–368. https://doi.org/10.1039/c003726e.

Withers, P., 2009. A review of observed variability in the dayside ionosphere of Mars. Adv. Space Res. 44, 277–307. https://doi.org/10.1016/j.asr.2009.04.027.

Withers, P., Morgan, D.D., Gurnett, D.A., 2015. Variations in peak electron densities in the ionosphere of Mars over a full solar cycle. Icarus 251, 5–11. https://doi.org/10.1016/j.icarus.2014.08.008.

Woods, T.N., Eparvier, F.G., 2006. Solar ultraviolet variability during the TIMED mission. Adv. Space Res. 37, 219–224. https://doi.org/10.1016/j.asr.2004.10.006.